Glabratephrin reverses doxorubicin resistance in triple negative breast cancer by inhibiting P-glycoprotein

Glabratephrin reverses doxorubicin resistance in triple negative breast cancer by inhibiting P-glycoprotein

Gamal Eldein Fathy Abd-ellatef[1,2], Elena Gazzano[1], Ahmed H. El-Desoky[3], Ahmed R. Hamed[4], Joanna Kopecka[1], Dimas Carolina Belisario[1], Costanzo Costamagna[1], Mohamed Assem S. Marie[5], Sohair R. Fahmy[5], Abdel-Hamid Z. Abdel-Hamid[2], Chiara Riganti[1]

1. Department of Oncology, University of Torino, via Santena 5/bis, 10126, Torino, Italy
2. Therapeutic Chemistry Department, Pharmaceutical and Drug Industries Research Division, National Research Centre, 33 El Bohouth St., 12622, Dokki, Giza, Egypt
3. Pharmacognosy Department, Pharmaceutical and Drug Industries Research Division, National Research Centre, 33 El Bohouth St., 12622, Dokki, Giza, Egypt
4. Chemistry of Medicinal Plants Department & Biology Unit of Central Laboratory, Pharmaceutical and Drug Industries Research Division, National Research Centre, 33 El Bohouth St., 12622, Dokki, Giza, Egypt
5. Zoology Department, Faculty of Science, Cairo University, Gamaa Street, Giza, Egypt

Corresponding author: Dr. Chiara Riganti, Department of Oncology, University of Torino, via Santena 5/bis, 10126, Torino, Italy; phone: +390116705857; fax:+390116705845; email: chiara.riganti@unito.it

Highlights

- Glabratephrin is a natural prenylated flavonoid from *Tephrosia purpurea*
- Glabratephrin reverses resistance to doxorubicin in triple negative breast cancer
- Glabratephrin binds P-glycoprotein and reduces its catalytic activity
- Glabratephrin is effective and safe in triple negative breast cancer xenografts

Graphical abstract

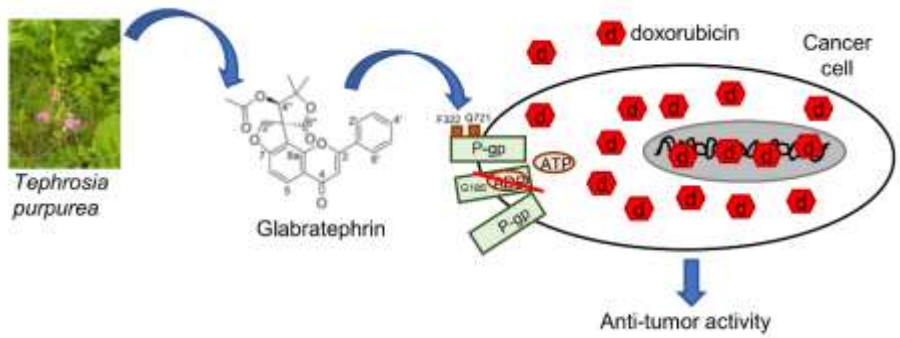

Abstract

Triple-negative breast cancer is one of the most aggressive breast cancer. The first therapeutic option is chemotherapy, often based on anthracycline as doxorubicin. However, chemotherapy efficacy is limited in by the presence of P-glycoprotein (Pgp), a membrane transporter protein that effluxes doxorubicin, reducing its cellular accumulation and toxicity. Inhibiting Pgp activity with effective and non-toxic products is still an open challenge.

In this work, we demonstrated that the natural product Glabratephrin (Glab), a prenylated flavonoid from *Tephrosia purpurea* with a unique chemical structure, increased doxorubicin accumulation and cytotoxicity in triple negative breast cancer cells with high levels of Pgp, characterized by both acquired or intrinsic resistance to doxorubicin. Glab also reduced the growth of Pgp-expressing tumors, without adding significant extra-toxicities to doxorubicin treatment. Interestingly, Glab did not change the expression of Pgp, but it reduced the affinity for Pgp and the efflux of doxorubicin, as suggested by the increased Km and the reduced Vmax. *In silico* molecular docking predicted that Glab binds two residues (phenylalanine 322, glutamine 721) localized in the transmembrane domains of Pgp, facing the extracellular environment. Moreover, site-directed mutagenesis identified glycine 185 as a critical residue mediating the reduced catalytic efficacy of Pgp elicited by Glab.

We propose Glab as an effective and safe compound able to reverse doxorubicin resistance mediated by Pgp in triple negative breast cancers, opening the way to a new combinatorial approach that may improve chemotherapy efficacy in the most refractory and aggressive breast cancer.

Keywords: Glabratephrin; P-glycoprotein; doxorubicin; triple negative breast cancer

Chemical compounds: doxorubicin (PubChem CID: 31703); Glabratephrin (PubChem CID: 12893624).

Abbreviations: MDR, multidrug resistance; ABCB1/Pgp: ATP binding cassette sub-family B1/P-glycoprotein; Dox, doxorubicin; ABCC1/MRP1: ATP binding cassette sub-family C1/multidrug resistance-associated protein 1 (MRP1); ABCG2/BCRP: ATP binding cassette sub-family G2/breast cancer resistance protein; QSAR: quantitative structure-activity relationships; Glab: Glabratephrin; FBS: fetal bovine serum; HIF-1α: Hypoxia-inducible factor-1α; CI: Combination Index; LDH: lactate dehydrogenase; AST: aspartate aminotransferase; ALT: alanine aminotransferase; AP: alkaline phosphatase; CPK: creatine phosphokinase; cTnI/T: cardiac troponin I/T; Pi: phosphate; MOE: Molecular Operating Environment; RMSD: root mean square deviation; ANOVA: analysis of variance; Gln: glutamine; Phe: phenylalanine; Gly: glycine; Val: valine; Ser: serine; Asn; asparagine; Ala: alanine; Thr: threonine; CS: collateral sensitivity; NBD: nucleotide binding domain; TMD: transmembrane domain; DSPE-PEG: distearoyl-phosphatidylethanolamine-polyethylene glycol.

1. Introduction

Multi-drug resistance (MDR) is a major cause of chemotherapy failure. One of the main mechanisms of chemoresistance is the high expression of adenosine triphosphate-binding cassette sub-family B1 (ABCB1)/P-glycoprotein (Pgp) that determines resistance to a broad spectrum of drugs used against breast cancer [1]. Doxorubicin (Dox), a typical substrate of Pgp [2], is an anthracycline extensively used to treat hematological and solid tumors, including triple negative breast cancer [3, 4]. Some of the last generation of Pgp inhibitors, such as Tariquidar and Elacridar, have enhanced the efficacy of anticancer drugs in preclinical studies, opening the perspective to their possible clinical use in patients with refractory breast cancers. While no Phase I/II trials based on Elacridar were registered, two trials using Tariquidar started (https://clinicaltrials.gov/) [5]. The phase-II NCT00048633 trial tested the efficacy of Tariquidar in combination with anthracyclines or taxanes in patients with advanced breast cancers, but it did not provide any conclusion about the clinical benefits derived from

this combination therapy. Similarly, no information about an increased efficacy of the combination of Tariquidar and vinorelbine were reported in the NCT00001944 trial. These data dampened the enthusiasm for setting larger phase III clinical trial with these two Pgp inhibitors. In addition, many Pgp inhibitors showed high toxicity [6]: the first-generation inhibitors of Pgp, such as verapamil, suffered of low therapeutic window and cardiotoxicity; the second-generation inhibitors displayed lower cardiotoxicity but often produced unwanted drug-drug interactions when administered with chemotherapeutic agents, limiting the efficacy of the latter [7]. Among the third-generation inhibitor, Elacridar induced modest neutropenia, Tariquidar was not associated with grade III/IV toxicities [7], but in both cases the lack of efficacy in terms of overall response rate limited the further clinical development. Finding effective and safe Pgp inhibitors remains still an open challenge.

In this scenario, natural products have been considered more and extensively as potential alternatives to synthetic molecules, although also natural compounds may suffer of the same drawbacks of synthetic compounds, as non-specific binding with the targets and/or unfavorable pharmacokinetic profiles [8]. The mechanisms at the basis of the reversion of chemoresistance by natural products are pleiotropic and sometimes not univocal, also in consideration of the wide range of natural compounds tested. Lipophilic terpenoids (e.g. monoterpenes, diterpenes, triterpenes, tetraterpenes), flavonoids, steroids such as cardiac glycosides, prenyl and steroid derivatives of quinolone and indole have been shown to inhibit Pgp, multidrug resistance-associated protein 1 (MRP1) and breast cancer resistance protein (BCRP) in a competitive manner [9], suggesting that these structures may fit the drug-binding pockets present on the different ABC transporters and displace the substrates. For more hydrophilic compounds with phenolic structure, it has been proposed that multiple H-bonds are formed with the protein, leading to the transporter's destabilization [9] and to non-competitive inhibition. Quercetin, catechins, morin and capsaicin, have been reported to inhibit Pgp more than other ABC transporters [10-12]. Quantitative structure-activity relationships (QSAR) studies highlighted those specific

moieties, such as a double bond between positions 2 and 3, a methoxyl group in position 3 and a hydroxyl group in position 5, that may confer this selectivity toward Pgp [12], leading to hypothesize that these moieties bind specific sites on Pgp, altering the substrates affinity or the tridimensional structure of the transporter, leading to a reduced catalytic efficacy. However, the effects of flavonoids are often tumor type- and model-dependent. For instance, in Pgp-expressing colon cancer the activity of quercetin, galangin and kaempferol on the efflux of adriamycin was unrelated to their structure, and all the compounds are very weak competitors [13]. Moreover, within the same tumor the efflux of adriamycin in crude membrane extracts of Pgp-expressing cells was significantly higher than the efflux measured in cell cultures [13], leading to hypothesize that other factors – as flavonoids uptake, change of Pgp structure in isolated membranes compared to living cells – impact on the final effect of flavonoids on chemoresistance. Flavonoids and terpenoids have broader effects than simply interacting with Pgp: for instance, they reduce the transcription of Pgp, inhibit the activity of cytochrome p450 isoforms catabolizing chemotherapeutic drugs, improve the pharmacokinetic profile of anti-cancer agents [12]. Overall, despite some contradictory findings, natural compounds with a flavonoid structure may be noteworthy of further investigation about their efficacy and safety as chemosensitizing agents, given their broad-spectrum effects on Pgp -expressing cells.

Tephrosia purpurea, a pantropical flowering plant of *Fabaceae* family widely used in traditional medicine, was reported to contain rotenoids, isoflavones, flavanones, flavones, flavanols and chalcones [14]. Prenylated flavonoids are the major isolated compounds from this plant. Among them Glabratephrin (Glab) was repeatedly isolated as the major constituent of *T. purpurea* [15-18]. Glab, and recently isoglabratephrin [15], are the only examples in nature of prenylated flavonoids with a 4-hydroxy-2,7-dioxaspiro[4.4]nonan-1-one-3,3-dimethyl ring moiety. Glab has shown multiple biological activities, ranging from anti-helmintic to anti-microbial, anti-fungal, anti-inflammatory, anti-pyretic effects [15-18]. The ethanolic extract of *T. purpurea* has shown cytotoxic activity against

the nasopharyngeal KB cell line, where it inhibits cell proliferation and migration [18]. Also Glabridin, a prenylated isoflavan with cyclic prenylation of ring A, is an anticancer agent [19] and a potent inhibitor of Pgp expression and activity [20], but no studies about the chemosensitizing properties of the rare spiro-prenylated compounds such as Glab and isoglabratephrin exist, despite QSAR studies predict that the prenylated flavonoid structure as that present in Glab may interact with Pgp [21]. Additionally, Glab was selected after a small-scale screening of 60 medicinal plant extracts and compounds from the library of the Pharmacognosy Department in National Research Center, Giza, Egypt, because it is extracted with a cost-effective isolation scheme that can fit industrial scale up. This is of paramount importance for eventual medicinal and clinical applications.

The aim of this work was to set up a combinatorial treatment based on Glab and Dox, able to reverse the resistance to this chemotherapeutic drug without unwanted systemic toxicity. We addressed this issue by testing the efficacy of Glab in triple negative breast cancer cells expressing different amount of Pgp, with an acquired or a constitutive resistance to Dox. In particular, we investigated the safety and ability of Glab in restoring the efficacy of Dox, the first-line treatment for triple negative breast cancer [22], in vitro and in vivo.

2. Materials and Methods

2.1. Chemicals and Materials

The lab supplies for cell cultures were obtained from Falcon (Becton Dickinson, Franklin Lakes, NJ). The electrophoresis reagents were from Bio-Rad Laboratories (Hercules, CA). The protein content of cell lysates was assessed with the BCA kit from Sigma Chemicals Co. (St. Louis, MO). Unless specified otherwise, all reagents were purchased from Sigma Chemicals Co.

2.2. Plant material

The aerial parts of *T. purpurea* were collected in February 2010, Marfai Valley, Gabal Elba, Egypt (22.2145 N, 36.3899 E, 450 m altitude). A voucher specimen has been deposited in the herbarium of

National Research Centre, Cairo, Egypt. The plant was identified by one of the authors (A. H. H. E). The plant was air-dried in the dark, reduced to a 36 mesh-powder using a cutter mill and kept in tightly sealed containers until the extraction.

2.3. Extraction and isolation of glabratephrin

Air-dried aerial plant powder (1200 g) was extracted with methylene dichloride (CH_2Cl_2)-methanol (MeOH) (1:1, 3 L) by maceration at room temperature and repeated 20 min cycles of sonication (50% amplitude; Hielscher UP200S, Ultrasound Sonicator, GmbH, Teltow, Germany). The solvent was evaporated under vacuum at 40°C. The residue (70 g) was subjected to silica gel open column chromatography (Silica gel 60 - 0.063-0.200 mm, 70-230 mesh -, Merck, Darmstadt, Germany) and eluted with *n*-hexane, ethyl acetate (EtOAc), with increasing polarity gradient from 10% to 100% EtOAc, then washed with MeOH. Similar fractions were pooled based on their separation by thin layer chromatography (TLC), carried out on TLC Silica gel 60G F_{254} 25 Glass plates (Merck), to yield 9 main fractions (FrA1-FrA9). FrA7 contained a major spot at R_f 0.5, emitting a blue fluorescence at 254 nm, and was subjected to silica gel column chromatography, eluted with *n*-hexane-EtOAc (2:1) to yield 12 fractions (FrB1-FrB12). The 11^{th} fraction, containing the major spot, was further purified by Sephadex LH-20 column chromatography (GE Healthcare Bio-Sciences AB, Uppsala, Sweeden), eluted with CH_2Cl_2–methanol (MeOH) (1:1) to yield 94 mg of colorless crystals that were identified as Glab (Figure 1), by ESIMS and ^{1}H-NMR analyses, whose spectrum (Supplementary Figure S1) matched with the already published spectra of Glab [18]. The purity of the compound was 99%.

2.3. Cell lines

Human triple negative breast cancer MDA-MB-231 cells and murine mammary JC cells were purchased from ATCC (Manassas, VA), and were cultured in RPMI-1640 medium with 10% fetal bovine serum (FBS) and 1% penicillin-streptomycin (PS). MDA-MB-231/DX were generated by culturing parental MDA-MB-231 cells in complete medium, adding Dox at increasing concentrations

every 5 passages (p0: 10 nM Dox; p5: 25 nM; p10: 50 nM; p15: 100 nM; p20: 250 nM; p25: 500 nM; p30: 1000 nM). Human peripheral blood mononuclear cells (PBMC) from 3 different healthy donors were obtained by the Blood Bank of AOU Città della Salute e della Scienza, Torino, Italy (#DG-767/2015) and cultured in RPMI-1640 medium with 10% FBS, 1% PS. Human fibroblasts were a kind gift of Prof. Francesco Novelli, Department of Molecular Biotechnology and Health Sciences, University of Torino, Italy, and were maintained in DMEM medium with 10% FBS, 1% PS.

2.4. Immunoblotting

Cells were rinsed with ice-cold lysis buffer (50 mM Tris, 10 mM EDTA, 1% v/v Triton-X100), supplemented with the protease inhibitor cocktail set III (80 μM aprotinin, 5 mM bestatin, 1.5 mM leupeptin, 1 mM pepstatin; Calbiochem, San Diego, CA), 2 mM phenylmethylsulfonyl fluoride and 1 mM Na_3VO_4. Samples were sonicated (with 10 bursts of 1 s, amplitude 40%; Hielscher UP200S, Ultrasound Sonicator) and centrifuged at 13,000 × g for 10 min at 4°C. 20 μg protein extracts were subjected to SDS-PAGE and probed with the following antibodies: anti-Pgp (1:250, rabbit polyclonal #sc-8313, Santa Cruz Biotechnology Inc., Santa Cruz, CA), anti-MRP1 (1:500, mouse clone MRPm5, Abcam, Cambridge, UK), anti-BCRP (1:500, mouse clone BXP-21, Santa Cruz Biotechnology Inc.), anti-β-tubulin (1:1000, mouse clone D10, Santa Cruz Biotechnology Inc.), followed by a peroxidase-conjugated secondary antibody (Bio-Rad Laboratories). The membranes were washed with Tris-buffered saline-Tween 0.1% v/v solution, the proteins were detected by enhanced chemiluminescence (Bio-Rad Laboratories). The relative quantitation of immunoblot was performed with the ImageJ software (https://imagej.nih.gov/ij/). The band density of untreated MDA-MB-231 cells was considered as 1 arbitrary unit.

2.5. RT-PCR

Total RNA was extracted and reverse-transcribed using the iScript™ cDNA Synthesis Kit (Bio-Rad Laboratories). qRT-PCR was performed using the IQ™ SYBR Green Supermix (Bio-Rad

Laboratories). The PCR primer sequences, designed using the qPrimerDepot software (http://primerdepot.nci.nih.gov/), were: *Pgp* (human): 5'-TGCTGGAGCGGTTCTACG-3', 5'-ATAGGCAATGTTCTCAGCAATG-3'; *S14* (human): 5'-CGAGGCTGATGACCTGTTCT-3', 5'-GCCCTCTCCCACTCTCTCTT-3'. The relative gene expression levels were calculated using the Gene Expression Quantitation software (Bio-Rad Laboratories).

2.6. Hypoxia Inducible Factor-1α (HIF-1α) activity

Nuclear proteins were extracted using the Nuclear Extract Kit (Active Motif, Rixensart, Belgium), and quantified. The activity of HIF-1α was assessed on 10 µg of nuclear proteins by the TransAM™ HIF Activity kit (Active Motif). The absorbance at 450 nm was measured with a Packard EL340 microplate reader (Bio-Tek Instruments, Winooski, VT). For each set of experiments, a blank was prepared with bis-distilled water, and its absorbance was subtracted from that obtained in the presence of nuclear extracts. Data were expressed as absorbance units/mg nuclear proteins.

2.7. Intracellular doxorubicin accumulation

Cells were washed twice with PBS 1X, detached by gentle scraping and centrifuged at 13,000 × g for 5 minutes at 4°C. Cell pellets were re-suspended in 400 µl of a 1:1 mixture of ethanol/0.3 N HCl and sonicated (10-sec bursts). The protein content was assessed with the BCA kit. The amount of intracellular doxorubicin was detected using a Synergy HT 96-well micro-plate reader (Bio-Tek Instruments). Excitation and emission wavelengths were 475 and 553 nm, respectively. A blank was prepared in the absence of cells in each set of experiments; its fluorescence was subtracted from that measured in each sample. Fluorescence was converted in nmoles doxorubicin/mg cell proteins using a calibration curve**.**

2.8. Cell viability

Cell viability was evaluated by crystal violet staining, as reported previously [23]. To calculate the IC_{50}, 1×10^4 cells were seeded in 96-well plates, treated with scalar concentrations (from 10^{-9} M to

10^{-2} M) of Glab for 72 h, and then stained with crystal violet solution. The quantitation of crystal violet staining was performed by reading the absorbance at 540 nm with a Synergy HT 96-well micro-plate reader (Bio-Tek Instruments). The mean absorbance of untreated cells was considered 100%; the absorbance units of the other experimental conditions were expressed as percentage of viable cells vs. untreated cells. IC_{50}, i.e. the concentration of the compound that decreases cell viability by 50%, was calculated with the GraphPad Prism (v 6.01) software. The Combination Index (CI) was calculated by measuring the viability in cells incubated with scalar concentrations (from 10^{-10} M to 10^{-5} M) of Dox and Glab, using the CalcuSyn software (www.biosoft.com/w/calcusyn.htm).

2.9. In vivo tumor growth

1×10^7 JC cells were mixed with 100 µl Matrigel and orthotopically implanted in 6-week-old female immunocompetent balb/C mice (Charles River Laboratories Italia, Calco), housed (5 per cage) under 12 h light/dark cycle, with food and drinking provided *ad libitum*. Tumor growth was measured daily by caliper, according to the equation $(LxW^2)/2$, where L=tumor length and W=tumor width. When tumors reached the volume of 50 mm^3, mice (n= 8/group) were randomized in the following groups and treated on day 1, 7, 14 after randomization as reported: 1) vehicle group, treated with 200 µl saline solution intravenously (i.v.); 2) Glabratephrin group, treated with a 200 µl water/10% DMSO solution i.v., containing 5 µM Glab; 3) doxorubicin group, treated with 5 mg/kg Dox, dissolved in 200 µl water i.v.; 4) Glabratephrin + doxorubicin group, treated with 100 µl of saline solution i.v. containing 5 µM Glab + 100 µl water solution containing 5 mg/kg Dox. Tumor volumes were monitored daily. Animals were euthanized at day 21 after randomization with zolazepam (0.2 ml/kg) and xylazine (16 mg/kg). Tumors were excised, photographed, fixed in 4% v/v paraformaldehyde overnight, and paraffin embedded. The paraffin sections were stained with haematoxylin-eosin or immune-stained for Ki67 (1:100; rabbit #AB9260, Sigma-Aldrich, St. Louis, MO), as index of cell proliferation, followed by a peroxidase-conjugated secondary antibody (1:100, Dako, Glostrup,

Denmark). Liver, kidneys and spleen were excised, fixed, and paraffin sections were examined after haematoxylin-eosin staining. The sections were examined with a Leica DC100 microscope (Leica, Weitzlar, Germany). Lactate dehydrogenase (LDH), aspartate aminotransferase (AST), alanine aminotransferase (ALT), alkaline phosphatase (AP), creatinine, creatine phosphokinase (CPK) and CPK-MB, cardiac troponin I (cTnI) and T (cTnT) were measured on blood samples collected immediately after euthanasia, using commercially available kits from Beckman Coulter Inc. (Beckman Coulter, Miami, FL). To test the acute toxicity, 6-week-old female balb/C mice (n=5/group) were treated with vehicle (200 µl saline solution i.v.) or with a 200 µl water/10% DMSO solution containing 0.5, 1, 5, 10 µM Glab (i.v.) After 24 h the animals were sacrificed, the blood was collected and the hematochemical parameters indicated above were assessed. In all studies, researchers analyzing the results were unaware of the treatments received by animals. The Animal care and experimental procedures were approved by the Bio-Ethical Committee of the Italian Ministry of Health (#122/2015-PR).

2.10. Rhodamine 123 efflux

Cells were washed with PBS, detached and re-suspended in 1 ml of fresh medium containing 5% FBS. The samples were maintained at 37°C for 20 min in the presence of 1 µg/ml Rhodamine 123. After this incubation time, cells were washed and re-suspended in 0.5 ml of PBS. The intracellular Rhodamine 123 content, which is inversely related to its efflux, was detected fluorimetrically using a a Synergy HT 96-well micro-plate reader (Bio-Tek Instruments). Excitation and emission wavelengths were 475 and 553 nm, respectively [24]. A blank was prepared in the absence of cells in each set of experiments; its fluorescence was subtracted from that measured in each sample. The results were expressed as nmoles/mg cell proteins.

2.11. Doxorubicin efflux

Cells were incubated for 10 min with increasing concentrations (0-50 μM) of Dox, with or without Glab, then washed and analyzed for the intracellular concentration of Dox. A second series of dishes, after the incubation under the same experimental conditions, were left for further 10 min at 37°C, then washed and tested for the intracellular drug content. The difference of Dox concentration between the two series during this time (dc/dt) was plotted versus the initial drugs concentration [24]. Values were fitted to Michaelis-Menten equation to calculate Vmax and Km, using the Enzfitter software (Biosoft Corporation, Cambridge, United Kingdom).

2.12. Pgp ATPase activity

The Pgp ATPase activity was measured in membrane vesicles as described previously [24]. Cells were washed with Ringer's solution (148.7 mM NaCl, 2.55 mM K_2HPO_4, 0.45 mM KH_2PO_4, 1.2 mM $MgSO_4$; pH 7.4), lysed on ice with lysis buffer (10 mM Hepes/Tris, 5 mM EDTA, 5 mM EGTA, 2 mM dithiothreitol; pH 7.4) supplemented with 2 mM phenylmethylsulfonyl fluoride, 1 mM aprotinin, 10 μg/ml pepstatin, 10 μg/ml leupeptin, and subjected to nitrogen cavitation at 1200 psi for 20 min. Samples were centrifuged at 300 × g for 10 min in the pre-centrifugation buffer (10 mM Tris/HCl, 25 mM sucrose; pH 7.5), overlaid on a sucrose cushion (10 mM Tris/HCl, 35% w/v sucrose, 1 mM EDTA; pH 7.5) and centrifuged at 14,000 × g for 10 min. The interface was collected, diluted in the centrifugation buffer (10 mM Tris/HCl, 250 mM sucrose; pH 7.5), centrifuged at 100,000 × g for 45 min. The vesicle pellet was re-suspended in 0.5 ml centrifugation buffer and stored at -80°C until the use, after the quantification of the protein content. 20 μg of total protein were incubated for 30 min at 37°C with 50 μl of the reaction mix (25 mM Tris/HCl, 3 mM ATP, 50 mM KCl, 2.5 mM $MgSO_4$, 3 mM dithiothreitol, 0.5 mM EGTA, 2 mM ouabain, 3 mM NaN_3; pH 7.0). In each set of experiments, a blank containing 0.5 mM Na_3VO_4 was included. The reaction was stopped by adding 0.2 ml ice-cold stopping buffer (0.2% w/v ammonium molybdate, 1.3% v/v H_2SO_4, 0.9% w/v SDS, 2.3% w/v trichloroacetic acid, 1% w/v ascorbic acid). After 30 min incubation at room temperature, the

absorbance of the phosphate hydrolyzed from ATP was measured at 620 nm, using a Packard EL340 microplate reader (Bio-Tek Instruments). The absorbance was converted into nmoles hydrolyzed phosphate (Pi)/min/mg proteins, according to the titration curve previously prepared.

2.13. Docking studies

The Molecular Operating Environment (MOE) software (Chemical Computing Group; https://www.chemcomp.com/Products.htm) was used to model the binding of Glab with Pgp (Protein Data Bank, PDB: 4M2S and 5KPI, as second crystal structure of mouse native Pgp showing 99% homology with 4M2S, according to Clustalw-multiple sequence alignment) [25]. The binding sites for QZ59-RRR, a cyclic-tris-(R)-valineselenazole, QZ59-SSS and verapamil, as well as the amino acid residues involved in binding, identified by Aller et al [26], were used for docking these compounds and Glab. Since 4M2S was co-crystalized with QZ59-RRR as a binding ligand, providing a necessary tool for comparing the binding affinity of unknown compounds as Glab with the reference compound, 4M2S was chosen for molecular docking study.

London ΔG scoring function was used for scoring. It was enhanced by using two different refinement methods - the force-field and Grid-Min poses - to ensure that refined poses satisfy the specified conformations. Rotatable bonds were allowed. The best 10 poses were retained and analyzed for the binding poses best score. The database browser was used in MOE to compare the docking poses to the ligand in the co-crystallized structure and to get the root mean square deviation (RMSD) of the docking pose compared to the co-crystallized ligand position.

The molecule builder tool of MOE software was used to construct a tridimensional model of the structures. Energy minimization was done through force-field MMFF94x optimization using a gradient of 0.0001 for determining low-energy conformations with the most favorable (lowest energy) geometry. The crystal structures of 4M2S receptor protein in complex with QZ59-RRR were obtained from the PDB.

Hydrogen atoms and partial charges were added to the protein to assign ionization states and position hydrogen atoms in the macromolecular structure. The binding free energy as well as hydrogen bonding were used to rank the binding affinity of QZ59-RRR and Glab to Pgp. The evaluation of the hydrogen bonds was done by measuring the hydrogen bond length, which did not exceed 3.5 Å. The RMSD of the docking pose compared to the co-crystal ligand position was used in the ranking. The mode of interaction of the native ligand within the crystal structure was used as a standard docked model as well as for RMSD calculation.

2.14. Overexpression of wild-type and mutated Pgp

The pHa vector containing the full-length *mdr1* cDNA, encoding for Pgp, was purchased from Addgene (Cambridge, MA) and subcloned into pCDNA3 vector. By sequencing the *mdr1* gene present in the pCDNA3 vector, we verified that it contained the wild-type sequence of Pgp (data not shown). pCDNA3 vector containing the wild-type *mdr1* cDNA, was subjected to PCR-based mutagenesis using the QuikChange kit (Stratagene, La Jolla, CA), following the manufacturer's instructions to generate the mutated constructs Gly185Val, Ser400Asn, Gly412Ala, Ser893Ala, Ser893Thr. The mutations were confirmed by DNA sequencing [27]. In transfection experiments, 5×10^4 cells were seeded in FBS-free medium and treated with 6 µl of jetPEI transfection reagent (Polyplus-transfection SA BIOPARC, Illkirch, France) and 3 µg DNA empty-pCDNA3 (mock cells), wild-type *mdr1*-pCDNA3 (wild-type Pgp) or mutated *mdr1*-pCDNA3 (mutated Pgp). After 6 h, cells were washed and grown in complete medium for 48 h before the experiments indicated in the Results section.

2.15. Statistical analysis

Results were analyzed by a one-way analysis of variance (ANOVA) and Tukey's test, using GraphPad Prism software (v 6.01). $p < 0.05$ was considered significant. All data were expressed as means $\pm$ SD.

3. Results

3.1. Doxorubicin accumulation in sensitive and resistant breast cancer cells

From triple negative breast cancer MDA-MB-231 cells, we generated the MDA-MB-231/DX variant by culturing parental cells in medium with increasing concentrations of doxorubicin, as detailed in the Materials and Methods section, to obtain a cellular model of acquired resistance to Dox. Murine mammary JC cells were used as a model of cells constitutively expressing Pgp and constitutively resistant to Dox [28]. Starting from passage number 10, MDA-MB-231/DX subline increased Pgp mRNA (Figure 2A) and protein (Figure 2B-C), reaching a plateau level at passage 20, corresponding to culture conditions in a medium containing 250 nM Dox. Pgp increase was not accompanied by any increase in MRP1 or BCRP (Figure 2B-C), two other transporters involved in Dox efflux [29]. The increase in Pgp expression was accompanied by a progressive increase in the activity of HIF-1α (Figure 2D), a transcription factor activated by Dox [30] and an inducer of Pgp gene transcription [31]. The same event was previously reported in the colon cancer HT29/DX subline, generated by culturing parental cell in medium with increasing concentration of Dox [32], suggesting that it is a process common to different cancer cell types during the acquisition of resistance.

For all the subsequent experiments, we used cells at passage 25, i.e. stably growing in medium containing 500 nM Dox. As shown in Figure 3A-B, MDA-MB-231/DX cells had an intermediate level of Pgp between parental MDA-MB-231 and JC cells. Consistently, MDA-MB-231/DX cells retained significantly less Dox than parental MDA-MB-231 cells, and JC cells had the lowest accumulation of the drug (Figure 3C). In the drug accumulation assay, we tested the concentration of 5 μM Dox, i.e. the minimum concentration that discriminates sensitive from resistant cells in terms of intracellular drug retention and cytotoxicity [32], and 25 μM Dox, i.e. a concentration that is cytotoxic for most cell lines, except for strongly Pgp-expressing cells as JC [33], and corresponds to

the highest concentration displaying good solubility in cell culture medium. Consistently with the intracellular retention data, in viability assays, 5 µM Dox induced a significant reduction of MDA-MB-231 cells, that was less pronounced in MDA-MB-231/DX subline and absent in JC cells (Figure 3D). Similarly, 25 µM Dox, that was more accumulated within all cell lines except JC cells (Figure 3C), produced a moderate decrease of cell viability in MDA-MB-231/DX cells but it had no effects in JC cells (Figure 3D). This different behavior can be explained by the different expression levels of Pgp between MDA-MB-231, MDA-MB-231/DX and JC cells. Based on these results, we considered MDA-MB-231, MDA-MB-231/DX and JC cells as Dox-sensitive, moderately Dox-resistant and strongly Dox-resistant cells, respectively.

3.2. Glabratephrin increases doxorubicin-induced cytotoxicity in resistant cells at non-cytotoxic concentrations

To investigate the effect of Glab, we first calculated its IC_{50} in our models. While in Dox-sensitive cells, the IC_{50} value was higher than 1 mM, in Dox-resistant cells it was reduced below 250 µM (Table 1).

Table 1. IC_{50} (mM) of Glabratephrin in breast cancer cells

Compound	IC_{50} (mM)		
	MDA-MB-231	MDA-MB-231/DX	JC
Glabratephrin	> 1	0.236 ± 0.067 **	0.138 ± 0.042 **

1×10^4 cells were seeded in quadruplicates in 96-well plates, treated with scalar concentrations (from 10^{-9} M to 10^{-2} M) of Glab for 72 h. Cell viability was measured by crystal violet staining. IC_{50}, i.e. the concentration of Glab that decreased the cell viability by 50%, was calculated with the GraphPad Prism (v 6.01) software. Data are means ± SD (n = 4). MDA-MB-231/DX and JC cells vs. MDA-MB-231 cells: ** $p < 0.01$.

388 The preferential sensitivity of Pgp-expressing cells prompted us to investigate if Glab may act as an
389 adjuvant of chemotherapeutic drugs substrates of Pgp, as Dox. In a preliminary screening, we
390 incubated the three cell lines with different concentrations of Glab (1 nM, 10 nM, 100 nM, 1 µM, 10
391 µM), with and without sub-toxic Dox concentrations (0.05, 0.5 and 5 µM). Cell viability was
392 measured after 72 h. At all concentrations Glab alone reduced cell viability less than 20% (Figure 4A-
393 C). In Dox-sensitive MDA-MB-231 cells, Glab did not increase the cytotoxic effects of Dox (Figure
394 4A). In moderately Dox-resistant MDA-MB-231/DX cells, at all concentrations Dox reduced cell
395 viability no more than 20%, but Glab - associated with Dox - increased cell death starting from 10
396 nM concentration (Figure 4B). The cytotoxic effect was progressively stronger at increasing
397 concentrations of Glab and Dox. In highly Dox-resistant JC cells, Dox did not significantly reduce
398 cells viability, as expected. Interestingly, Glab rescued the cytotoxicity of Dox, starting from the
399 concentration of 100 nM; the number of viable cells was progressively reduced at the increasing of
400 Glab and Dox concentrations (Figure 4C). The effect of Glab and Dox was synergistic, as indicated
401 by the CI of 0.29721 in MDA-MB-231/DX cells (Figure 4D) and 0.10922 in JC cells (Figure 4E). To
402 evaluate the toxicity of the different combinations of Glab and Dox on non-transformed cells, we
403 measured the cell viability in human PBMC and fibroblasts. As reported in the new Supplementary
404 Figure S2A-B, the reduction in the viability of normal cells was comparable or lower than in breast
405 cancer cell lines.

406 *3.3. Glabratephrin reverses doxorubicin resistance in vivo without inducing systemic toxicities*

407 Prompted by the good anti-proliferative efficacy achieved against breast cancer cell lines and the
408 acceptable toxicity profile observed in non-transformed cells in vitro, we next evaluated the efficacy
409 of Glab in mice bearing JC tumors that were completely refractory to Dox (Figure 5A-B). In a
410 preliminary set of experiments to evaluate the acute toxicity, we determined that 5 µM Glab was the
411 maximal dose of the compound that did not cause liver, kidney or heart toxicities, based on the

hematochemical parameters (Supplementary Table S1). This concentration was chosen for the subsequent experiments of anti-tumor efficacy. While Glab alone did not have any effects, the combination of Glab + Dox lowered the rate of tumor growth (Figure 5A), resulting in smaller tumor masses (Figure 5B). The growth profile was characterized by an initial delay in the growth of tumor, followed by a steady-state in the tumor volumes. This trend suggests that the effect of Glab + Dox combination is cytostatic. In keeping with these results, the positivity for Ki67, an index of tumor proliferation, was similar in animals treated with vehicle, Glab or Dox alone, but it was reduced in the tumors from Glab + Dox group (Figure 5C), indicating a good antitumor efficacy of the combination.

We are aware that many Pgp inhibitors, particularly of first and second generation, were effective *in vitro* but they failed in preclinical models for the high systemic toxicity [34]. Post-mortem examination of liver, kidney and spleen did not show histological abnormalities in these organs for all the treatment groups, including the animals treated with Glab and Dox combination (Figure 5D). At the time of sacrifice, we also measured specific hematochemical parameters as indexes of possible systemic toxicities in the treated animals (Table 2). According to these parameters, no signs of liver toxicities - indicated by LDH, AST, ALT, AP - and kidney toxicities - indicated by creatinine - were detected in Glab-treated animals, alone or in combination with Dox, in agreement with the lack of histological abnormalities. In our experimental protocol, Dox was used at a the maximum tolerated dose [35]. This regimen did not induce fatal events in the treated animals, but it elicited an appreciable cardiac damage indicated by the increase of CPK and its cardiac specific isoform CPK-MB, as well as cTnT. Glab did not affect cardiac parameters when used alone nor worsened the damaged elicited by Dox when used in combination (Table 2), indicating that it did not exacerbate Dox cardiotoxicity.

Table 2. Hematochemical parameters of treated animals

	Ctrl	Glab	Dox	Glab + Dox
LDH (U/l)	6578 ± 504	6892 ± 298	6791 ± 471	6792 ± 561
AST (U/l)	193 ± 39	145 ± 35	139 ± 41	127 ± 38
ALT (U/l)	34 ± 7	36 ± 5	38 ± 7	39 ± 10
AP (U/l)	113 ± 31	145 ± 23	139 ± 18	128 ± 27
Creatinine (mg/l)	0.071 ± 0.012	0.065 ± 0.008	0.061 ± 0.008	0.064± 0.009
CPK (U/l)	287 ± 77	281 ± 62	542 ± 45 *	591 ± 78 *
CPK-MB (ng/ml)	0.128 ± 0.062	0.110 ± 0.044	0.321 ± 0.076 *	0.296 ± 0.081 *
cTnI (pg/ml)	1.089 ± 0.034	1.028± 0.089	1.055 ± 0.041	1.032 ± 0.042
cTnT (pg/ml)	1.983 ± 0.301	1.872 ± 0.217	2.986 ± 0.104 *	3.117 ± 0.285 *

Balb/C mice (n=8 animals/group) were treated as described in Figure 5. Blood was collected immediately after euthanasia and analyzed for lactate dehydrogenase (LDH), aspartate aminotransferase (AST), alanine aminotransferase (ALT), alkaline phosphatase (AP), creatinine, creatine phosphokinase (CPK) and CPK-MB, cardiac troponin I (cTnI) and T (cTnT). Data are presented as means ± SD. * $p < 0.05$: vs Ctrl group.

3.4. Glabratephrin increases intracellular doxorubicin accumulation and cytotoxicity in resistant breast cancer cells by decreasing Pgp activity

We next investigated whether Glab enhanced Dox cytotoxicity by increasing its intracellular retention and/or reducing Dox efflux via Pgp. After 24 h incubation with 5 µM Dox and 100 nM Glab, corresponding to the lowest concentration of Glab increasing the drug's cytotoxicity in both the resistant cell lines analyzed, Dox was significantly more accumulated in the Pgp-expressing MDA-MB-231/DX and JC cells, not in the Pgp-negative MDA-MB-231 cells (Figure 6A). Similarly, Glab

increased the retention of Rhodamine 123, another substrate of Pgp, in resistant cells, when co-incubated with the dye (Figure 6B). These data suggest that Glab may compete with Dox or Rhodamine 123 for their binding and efflux through Pgp.

To further explore this issue, we measured the kinetic parameters of Dox efflux from MDA-MB-231/DX and JC cells. As shown in Figure 6C and Table 3, MDA-MB-231/DX had a lower Vmax than JC cells, consistently with their lower expression of Pgp. In both cell lines, Glab reduced the Vmax of Dox efflux, suggesting that it decreased the maximal catalytic efficiency of Pgp. Our hypothesis was proved by the significant decrease of Pgp ATPase activity induced by Glab (Figure 6D). By contrast, Glab did not change the amount of Pgp protein (Supplementary Figure S3), suggesting that the reduction of Vmax was caused by a decreased activity of the transporter, not by a different expression. In parallel, Glab increased the Km of Dox (Figure 6C; Table 3), indicating a reduction in Dox affinity for Pgp.

Table 3. Kinetic parameters of Dox efflux

Cells	Vmax (µmoles/min)	Km (µM)
MDA-MB-231/DX - Glab	13.2 ± 2.4	0.15 ± 0.04
MDA-MB-231/DX + Glab	6.7 ± 1.2 ***	0.27 ± 0.05 **
JC - Glab	4.2 ± 0.7	0.12 ± 0.04
JC + Glab	1.9 ± 0.9 *	0.24 ± 0.04 **

Cells were incubated as reported in Figure 6C. Vmax and Km were calculated with the Enzfitter software. Data are presented as means ± SD (n = 3). Glab-treated vs. untreated cells: * $p < 0.05$; ** $p < 0.01$; *** $p < 0.001$.

3.5. Molecular docking studies of Glabratephrin on Pgp

Glab was docked at QZ59-RRR, QZ59-SSS and verapamil binding sites [26]. The docking scores - based on the binding affinity measured by RMSD values, on the predicted hydrogen bond and on the binding free energy (S-score) - were used to evaluate binding affinity. The docking scores in the binding site of QZ59-RRR were the only favorable for inhibitory activity of Glab. Applying the MOE software, Pgp (PDB: 4M2S) structure was separated from the structure of the putative ligand. The binding free energy as well as hydrogen bonding were used to rank the binding affinity of QZ59RRR and Glab to Pgp. Docking accuracy was validated by re-docking the co-crystallized ligand QZ59-RRR into the binding site of QZ59-RRR in Pgp (Figure 7A), with a RMSD of 1.31 Å and a binding free energy of −10.07 kcal/mol (Table 4).

Glab docking calculation was carried out using the standard default variable in the MOE software. Glab was docked into the same groove of the co-crystallized ligand QZ59-RRR (Figure 7B) and had a comparable binding free energy (Table 4). The refined docking of Glab to Pgp is reported in Figure 7C.

Table 4. Binding affinity evaluation using binding free energy

Ligand	**S- Score (Kcal/mol)**	**Number of H-bond involved**	**Aminoacids involved**
QZ59-RRR	-10.07	2	Gln 721; Phe 979
Glabratephrin	-10.95	2	Gln 721; Phe 332

Gln: glutamine; Phe: phenylalanine

The binding mode of QZ59-RRR with Pgp (Supplementary Figure S4) was predicted to have one H-bond donor with Gln721 at 3.2 Å distance and one arene interaction with Phe979 (Figure 8A). The binding mode of Glab with Pgp was predicted to have one H-bond donor with Gln721 at 2.6 Å distance and one arene interaction Phe332 (Figure 8B). These results suggest that both the carbonyl

485 group of the acetyl residue and the mono-substituted phenyl moiety of Glab are necessary to interact
486 with Pgp.

487 *3.6. The Pgp domain centered around glycine 185 is necessary to mediate Glabratephrin activity*

488 To identify a possible mechanism by which Glab, after binding Pgp, interferes with the catalytic
489 activity of the transporter, we over-expressed wild-type Pgp and five different mutants containing the
490 mutations mostly annotated in human tumors - Gly185Val, Ser400Asn, Gly412Ala, Ser893Ala,
491 Ser893Thr (ABCMDb/Database for Mutations in ABC proteins; http://abcmutations.hegelab.org/) in
492 MDA-MB-231 cells. As shown in Figure 9A, both wild-type and mutated Pgp were expressed at
493 comparable levels, higher than the levels of endogenous Pgp. Interestingly, Glab increased Dox
494 accumulation (Figure 9B) and ATPase activity (Figure 9C) in cells expressing wild-type Pgp and all
495 Pgp mutants, except in cells expressing Gly185Val-mutated protein (Figure 9B-C). These results
496 suggest that the domain containing Gly185 is important in determining the inhibitory effect of Glab
497 on Pgp activity.

498 **4. Discussion**

499 In this work, we reported for the first time the potential of Glab, a prenylated flavonoid extracted
500 from the medicinal plant *T. purpurea*, with a unique chemical structure, in reversing the resistance to
501 Dox mediated by Pgp in triple negative breast cancer cells.

502 A cytotoxic activity of Glab against oral cancer cells has been reported previously [14]. The IC_{50}
503 values measured in triple negative breast cancer cells, however, indicated that the compound reduced
504 cell viability only at high micromolar concentrations. Interestingly, IC_{50} values were lower when the
505 levels of Pgp increased, either in cells with acquired or constitutive resistance to Dox. The peculiar
506 cytotoxicity of a compound in cells highly expressing Pgp is known as “collateral sensitivity” (CS)
507 [36] and is considered the most effective way to eradicate MDR. Thiosemicarbazones, 1,10-

phenanthrolines, as well as natural-products such as sesquiterpenic benzoquinones and flavonoids, have been recently identified as potent inducers of CS [37]. According to the profile of IC_{50}, Glab is a potential CS-inducer since it is slightly more effective as cytotoxic agent in cells with high levels of Pgp, according to the IC_{50}. However, high micromolar concentrations, at which Glab resulted moderately cytotoxic, are difficult to be reached in vivo. Hence, we excluded that Glab is a potent anti-cancer agent when used alone.

On the other hand, Glab, in combination with Dox, exerted a synergistic toxicity against cells expressing Pgp. Consistently, in xenografts of highly Pgp-expressing/Dox-resistant breast cancers Glab rescued the anti-tumor efficacy of Dox. Besides exerting a strong reduction of tumor growth, the combination of Glab and Dox did not show toxicity, as suggested by in vitro assays on non-transformed cells, and *post-mortem* histological and hematochemical parameters of the treated animals. Moreover, given the significant decrease of tumor volume elicited by this combination, we propose Glab as an option to reduce the doses of Dox, preserving good efficacy against Pgp-expressing tumors and reducing the dose-dependent cardiotoxicity that is the major side-effects of anthracyclines.

Of note, the higher Pgp level was in triple negative breast cancer cells, the higher synergism between Glab and Dox was observed. To explain this synergistic effect in Pgp-expressing cells, we hypothesized that Glab may affect the expression or activity of Pgp, reducing the efflux of Dox. The kinetic parameters of Dox efflux revealed a higher Km and a lower Vmax, together with a decreased ATPase activity, in Pgp-expressing cells treated with Glab. By contrast, Glab did not change the expression of Pgp. Upon binding, several substrates including Dox trigger the ATP hydrolysis and the substrate transport [38]. Competitive Pgp inhibitors bind to the substrate binding sites and impair the substrate binding coupled with the ATP hydrolysis; non-competitive inhibitors bind to the transmembrane domains (TMD) of Pgp, to the intracellular linking domains or to the nucleotide

binding domains (NBD), impairing the catalytic cycle [38]. Our results pointed out that Glab competes with Dox for its efflux through Pgp. This may be due to the reduced binding and/or reduced release of Dox, indicated by the increased Km, and to the uncoupling of substrate binding, ATP hydrolysis and substrate efflux, indicated by the lower Vmax.

To deepen our knowledge about the potential binding sites of Glab on Pgp, we performed molecular docking studies and site-directed mutagenesis assays. According to the docking simulation, Glab is predicted to bind Phe332 and Gln721, two residues mapping in the Pgp TMD 1 and 2, facing the outer membrane leaflet [39]. They are outside the so-called hydrophobic pocket, i.e. the binding pocket most likely involved in Dox transport [40], which is localized at the interface between Pgp and inner membrane leaflet [41]. Therefore, it is unlikely that the increase in Dox Km induced by Glab was due to a decrease in the drug binding. We hypothesize that Glab may instead interfere with the Dox release or with the substrate-triggered ATP hydrolysis [38]. The results of site-directed mutagenesis indicated that Glab interferes with the domain centered around Gly185. This result is of particular interest in a pharmacological perspective. Indeed, among the mutations analyzed, Ser400 and Gly412 mutations have no reported clinical significance; these amino acids are in exons 12 and 13 that are components of the NBD at the N-terminal side of Pgp [42]. Ser893 is localized between the TMD 10 and 11 of Pgp; its mutation alters the efflux of lipophilic drugs, such as simvastatin [43], ondasetron [44] and paclitaxel [45] but not Dox. Gly185 is in a large hydrophobic domain of Pgp involved in drug release outside the cell [46]. Moreover, Gly185 dictates the conformation changes induced by ATP hydrolysis and culminating in the extracellular release of the drugs: its mutation into Val determines a more efficient coupling between these two processes [47]. Gly185Val mutation has been involved in the resistance to lipophilic drugs such as colchicine, epipodophyllotoxins [48] and Dox [24]. Moreover, this mutation impairs the effects of Pgp allosteric inhibitors, such as distearoyl-phosphatidylethanolamine-polyethylene glycol (DSPE-PEG), which increases the Km of Dox and

reduces the ATPase activity in wild-type Pgp, not in Gly185Val-mutated Pgp [24]. Of note, Glab shows the same properties of DSPE-PEG, since it increased Dox Km and decreased Pgp ATPase activity, but lose its efficacy in cells mutated at Gly185. We may hypothesize that the binding of Glab on TMD 1 and 2 alters the conformation of Gly185-centered domain and disrupts the efficient coupling between ATP hydrolysis and Dox efflux. In consequence of the decreased catalytic activity of Pgp, the release of Dox towards the external side is less efficient, as suggested by the increased Km of the drug and the reduced Vmax.

Dox is one of the first therapeutic option in triple negative breast cancer [22], but this type of breast cancer is less responsive to Dox than other breast cancer types [49]. One of the main reasons for the low success of Dox is the abundant presence of Pgp in triple negative breast cancer cells [50]. Increasing Dox efficacy in this setting is still an unmet need. Unluckily, most of the small molecules designed as Pgp inhibitors [34] or selective killers of Pgp-expressing cells [36, 37] were effective *in vitro* but not in preclinical models, because of low efficacy and/or undesired toxicities. Natural products structurally analogue to Glab may offer a safe and effective alternative to inhibit Pgp.

In this work, we identified Glab as a potent Dox-sensitizer in Pgp-expressing triple negative breast cancer cells, thanks to its inhibition of Pgp catalytic efficiency and Dox efflux. The increased intracellular retention of Dox determines an increased cytotoxicity *in vitro* and a significant reduction in tumor growth *in vivo*. Moreover, Glab did not display systemic toxicities according to the hematochemical and histological parameters measured. These results may open the way to further investigations of the efficacy of Glab in patient-derived triple negative breast cancer cells and xenografts, to identify subset of patients – unresponsive to Dox because of high levels of Pgp and characterized by poor prognosis – who may benefit from the use of Glab as a potentially adjuvant agent.

Disclosure of Potential Conflicts of Interest

None

Acknowledgments

The work was supported by the Italian Association for Cancer Research (AIRC; IG21408). Gamal Eldein Fathy Abd-ellatef (G.E.F.A.) was recipient of a joint PhD supervision mission from the Academy of Scientific Research and Technology in Egypt.

References

[1] M. Hugle, S. Czaplinski, K. Habermann, M. Vogler, S. Fulda. Identification of Smac mimetics as novel substrates for P-glycoprotein. Cancer Lett. 440–441 (2019) 126–134. https://doi.org/10.1016/j.canlet.2018.10.001.

[2] I.C. Salaroglio, E. Gazzano, J. Kopecka, K. Chegaev, C. Costamagna, R. Fruttero, S. Guglielmo, C. Riganti. New tetrahydroisoquinoline derivatives overcome Pgp activity in brain-blood barrier and glioblastoma multiforme in vitro. Molecules. 23 (6) (2018). https://doi.org/10.3390/molecules23061401.

[3] K. Chegaev, A. Fraix, E. Gazzano, G.E.F. Abd-Ellatef, M. Blangetti, B. Rolando, S. Conoci, C. Riganti, R. Fruttero, A. Gasco, S. Sortino. Light-regulated NO release as a novel strategy to overcome doxorubicin multidrug resistance. ACS Med. Chem. Lett. 8 (3) (2017) 361–365. https://doi.org/10.1021/acsmedchemlett.7b00016.

[4] Y.L. Franco, T.R. Vaidya, S. Ait-Oudhia. Anticancer and cardio-protective effects of liposomal doxorubicin in the treatment of breast cancer. Breast Cancer: Targets and Therapy (Dove Med Press). 10 (2018) 131–141. https://doi.org/10.2147/BCTT.S170239.

[5] https://clinicaltrials.gov/ (accessed on 20 October 2021)

[6] H. Thomas, H.M. Coley. Overcoming multidrug resistance in cancer: an update on the clinical strategy of inhibiting P-glycoprotein. Cancer Control. 10 (2) (2003) 159–165. https://doi.org/10.1177/107327480301000207.

[7] J.I. Lai, Y.I. Tseng, M.H. Chen, C.F. Huang, P.M. Chang. Clinical Perspective of FDA Approved Drugs With P-Glycoprotein Inhibition Activities for Potential Cancer Therapeutics. Front. Oncol. 10 (2020) 561936. https://doi.org/10.3389/fonc.2020.561936.

[8] S. Dallavalle, V. Dobričić, L. Lazzarato, E. Gazzano, M. Machuqueiro, I. Pajeva, I. Tsakovska, N. Zidar, R. Fruttero. Improvement of conventional anti-cancer drugs as new tools against multidrug resistant tumors. Drug Resist. Updat. 50 (2020) 100682. https://doi.org/10.1016/j.drup.2020.100682.

[9] M. Wink, M.L. Ashour, M.Z. El-Readi. Secondary metabolites from plants inhibiting ABC transporters and reversing resistance of cancer cells and microbes to cytotoxic and antimicrobial agents. Front. Microbiol. 3 (2012) 1–15. https://doi.org/10.3389/fmicb.2012.00130.

[10] S. Zhang, M.E. Morris. Effects of the flavonoids biochanin A, morin, phloretin, and silymarin on P-glycoprotein-mediated transport. J. Pharmacol. Exp. Ther. 304 (3) (2003) 1258–1267. https://doi.org/10.1124/jpet.102.044412.

[11] T. Nabekura, S. Kamiyama, S. Kitagawa. Effects of dietary chemopreventive phytochemicals on P-glycoprotein function. Biochem. Biophys. Res. Commun. 327 (3) (2005) 866–870. https://doi.org/10.1016/j.bbrc.2004.12.081.

[12] J. Yu, P. Zhou, J. Asenso, X.D. Yang, C. Wang, W. Wei. Advances in plant-based inhibitors of P-glycoprotein. J. Enzyme Inhib. Med. Chem. 31 (6) (2016) 867–881. https://doi.org/10.3109/14756366.2016.1149476.

[13] J.W. Critchfield, C.J. Welsh, J.M. Phang, G.C. Yeh. Modulation of adriamycin accumulation and efflux by flavonoids in HCT-15 colon cells. Activation of P-glycoprotein as a putative mechanism. Biochem Pharmacol. 48 (7) (1994) 1437–1445. https://doi.org/10.1016/0006-2952(94)90568-1.

[14] A. Pelter, R.S. Ward, E. V. Rao, N.R. Raju. 8-Substituted flavonoids and 3′-substituted 7-oxygenated chalcones from Tephrosia Purpurea. J. Chem. Soc. Perkin Trans. 1 (1981) 2491–2498. https://doi.org/10.1039/P19810002491.

[15] M.E.F. Hegazy, M.H. Abd El-Razek, F. Nagashima, Y. Asakawa, P.W. Paré. Rare prenylated

630 flavonoids from Tephrosia Purpurea. Phytochemistry. 70 (11–12) (2009) 1474–1477.
631 https://doi.org/10.1016/j.phytochem.2009.08.001.

632 [16] A.E.H.H. Mohamed, A.K. Khalafallah, A.H. Yousof. Biotransformation of glabratephrin, a rare
633 type of isoprenylated flavonoids, by Aspergillus niger. Zeitschrift fur Naturforsch. - Sect. C J. Biosci.
634 63 (7–8) (2008) 561–564. https://doi.org/10.1515/znc-2008-7-816.

635 [17] M.I. Ammar, G.E. Nenaah, A.H.H. Mohamed. Antifungal activity of prenylated flavonoids
636 isolated from Tephrosia apollinea L. against four phytopathogenic fungi. Crop Prot. 49 (2013) 21–25.
637 https://doi.org/10.1016/j.cropro.2013.02.012.

638 [18] R. Vleggaar, G.J. Kruger, T.M. Smalberger, A.J. Van Den Berg. Flavonoids from Tephrosia—
639 XI1: The structure of glabratephrin. Tetrahedron. 34 (9) (1978) 1405–1408.
640 https://doi.org/10.1016/0040-4020(78)88338-0.

641 [19] C.T. Chen, Y.T. Chen, Y.H. Hsieh, C.J. Weng, J.C. Yeh, S.F. Yang, C.W. Lin, J.S. Yang.
642 Glabridin induces apoptosis and cell cycle arrest in oral cancer cells through the JNK1/2 signaling
643 pathway. Environ. Toxicol. 33 (6) (2018) 679-685. https://doi.org/10.1002/tox.22555.

644 [20] J. Qian, M. Xia, W. Liu, L. Li, J. Yang, Y. Mei, Q. Meng, Y. Xie. Glabridin resensitizes p-
645 glycoprotein-overexpressing multidrug-resistant cancer cells to conventional chemotherapeutic
646 agents. Eur. J. Pharmacol. 852 (2019) 231-243. https://doi.org/10.1016/j.ejphar.2019.04.002.

647 [21] J. Molnar, N. Gyemant, M. Tanaka, J. Hohmann, E. Bergmann-Leitner, P. Molnár, J. Deli, R.
648 Didiziapetris, M.J. Ferreira. Inhibition of multidrug resistance of cancer cells by natural diterpenes,
649 triterpenes and carotenoids. Curr. Pharm. Des. 12 (3) (2006) 287–311.
650 https://doi.org/10.2174/138161206775201893

651 [22] B. Székely, A. L. M. Silber, L. Pusztai. New therapeutic strategies for triple-negative breast

652 cancer. Oncology (Williston Park). 31 (2) (2017) 130–137.

653 [23] C. Riganti, J. Kopecka, E. Panada, S. Barak, M. Rubinstein. The role of C/EBP-β LIP in
654 multidrug resistance. J Natl Cancer Inst. 107 (5) (2015) pii: djv046. doi: 10.1093/jnci/djv046.

655 [24] J. Kopecka, G. Salzano, I. Campia, S. Lusa, D. Ghigo, G. De Rosa, C. Riganti. Insights in the
656 chemical components of liposomes responsible for P-glycoprotein inhibition. Nanomedicine. 10 (1)
657 (2014) 77–87. https://doi.org/10.1016/j.nano.2013.06.013.

658 [25] L. Esser, F. Zhou, K.M. Pluchino, J. Shiloach, J. Ma, W. K. Tang, T. Zhou,. Structures of the
659 multidrug transporter P-glycoprotein reveal asymmetric ATP binding and the mechanism of
660 polyspecificity. J. Biol. Chem. 292 (2) (2017) 446-461.

661 [26] S.G. Aller, J. Yu, A. Ward, Y. Weng, S. Chittaboina, R. Zhuo, *et al.* Structure of P-glycoprotein
662 reveals a molecular basis for poly-specific drug binding Science, 323 (2009), pp. 1718-1722

663 [27] C. Riganti, C. Voena, J. Kopecka, P. A. Corsetto, G. Montorfano, E. Enrico, C. Costamagna, A.
664 M. Rizzo, D. Ghigo, A. Bosia. Liposome-encapsulated doxorubicin reverses drug resistance by
665 inhibiting P-glycoprotein in human cancer cells. Mol. Pharm. 8 (3) (2011) 683–700.
666 https://doi.org/10.1021/mp2001389.

667 [28] B. D. Lee, K. J. French, Y. Zhuang, C. D. Smith. Development of a syngeneic in vivo tumor
668 model and its use in evaluating a novel P-glycoprotein modulator, PGP-4008. Oncol. Res. 14 (1)
669 (2003) 49–60.

670 [29] M. M. Gottesman, T. Fojo, S. E. Bates. Multidrug resistance in cancer: Role of ATP–dependent
671 transporters. Nat. Rev. Cancer. 2 (1) (2002) 48–58. https://doi.org/10.1038/nrc706.

672 [30] J. Kopecka, I. Campia, A. Jacobs, A. P. Frei, D. Ghigo, B. Wollscheid, C. Riganti. Carbonic
673 anhydrase XII is a new therapeutic target to overcome chemoresistance in cancer cells. Oncotarget. 6

(9) (2015) 6776–6793. https://doi.org/10.18632/oncotarget.2882.

[31] K. M. Comerford, T. J. Wallace, J. Karhausen, N. A. Louis, M. C. Montalto, S. P. Colgan,. Hypoxia-Inducible Factor-1-dependent regulation of the multidrug resistance (MDR1) gene. Cancer Res. 62 (12) (2002) 3387–3394.

[32] C. Riganti, E. Miraglia, D. Viarisio, C. Costamagna, G. Pescarmona, D. Ghigo, A. Bosia,. Nitric oxide reverts the resistance to doxorubicin in human colon cancer cells by inhibiting the drug efflux. Cancer Res. 65 (2) (2005) 516–525.

[33] C. Riganti, E. Gazzano, G.R. Gulino, M. Volante, D. Ghigo, J. Kopecka,. Two repeated low doses of doxorubicin are more effective than a single high dose against tumors overexpressing P-glycoprotein. Cancer Lett. 360 (2015) 219-226. https://doi.org/10.1016/j.canlet.2015.02.008.

[34] R. Callaghan, F. Luk, M. Bebaw. Inhibition of the multidrug resistance P-glycoprotein: time for a change of strategy? Drug Metab. Dispos. 42 (4) (2014) 623–631. https://doi.org/10.1124/dmd.113.056176.

[35] E. Gazzano, B. Rolando, K. Chegaev, I. C. Salaroglio, J. Kopecka, I. Pedrini, S. Saponara, M. Sorge, I. Buondonno, B. Stella, A. Marengo, M.Valoti, M. Brancaccio, R. Fruttero, A. Gasco, S. Arpicco, C. Riganti. Folate-targeted liposomal nitrooxy-doxorubicin: an effective tool against P-glycoprotein-positive and folate receptor-positive tumors. J. Control. Release. 270 (2018) 37–52. https://doi.org/10.1016/j.jconrel.2017.11.042.

[36] K. M. Pluchino, M. D. Hall, A. S. Goldsborough, R. Callaghan, M. M. Gottesman. Collateral sensitivity as a strategy against cancer multidrug resistance. Drug Resist. Updat. 15 (1–2) (2012) 98–105. https://doi.org/10.1016/j.drup.2012.03.002.

[37] G. Szakács, M. D. Hall, M. M. Gottesman, A. Boumendjel, R. Kachadourian, B. J. Day, H.

Baubichon-Cortay, A. Di Pietro. Targeting the Achilles heel of multidrug-resistant cancer by exploiting the fitness cost of resistance. Chem Rev. 114 (11) (2014) 5753–5774. https://doi.org/10.1021/cr4006236.

[38] J. Dong, Z. Qin, W.D. Zhang, G. Cheng, Y.G. Assaraf, C.R. Ashby, Z.S. Chen, X.D. Cheng, J.J. Qin. Medicinal chemistry strategies to discover P-glycoprotein inhibitors: An update. Drug Resist. Updat. 49 (2020) 100681. doi: 10.1016/j.drup.2020.100681

[39] T.W. Loo, D.M. Clarke. Mapping the binding site of the inhibitor tariquidar that stabilizes the first transmembrane domain of P-glycoprotein. J. Biol. Chem. 290 (49) (2015) 29389–29401. doi:10.1074/jbc.M115.652602

[40] I.K. Pajeva, M. Wiese. Structure-activity relationships of tariquidar analogs as multidrug resistance modulators. AAPS J. 11 (2009) 435-444. doi:10.1208/s12248-009-9118-z.

[41] Q. Qu, F. Sharom. Proximity of bound Hoechst 33342 to the ATPase catalytic sites places the drug binding site of P-glycoprotein within the cytoplasmic membrane leaflet. Biochemistry. 41 (2002) 4744–52. doi:10.1021/bi0120897

[42] M. Raymond, P. Gross. Mammalian multidrug-resistance gene: correlation of exon organization with structural domains and duplication of an ancestral gene. Proc. Natl. Acad. Sci. U. S. A. 86 (17) (1989) 6488–6492. https://doi.org/10.1073/pnas.86.17.6488.

[43] M. L. Becker, L. E. Visser, R. H. N. Van Schaik, A. Hofman, A. G. Uitterlinden, B. H. Stricker. Common genetic variation in the ABCB1 gene is associated with the cholesterol-lowering effect of simvastatin in males. Pharmacogenomics. 10 (11) (2009) 1743–1751. https://doi.org/10.2217/pgs.09.105.

[44] E. M. Choi, M. G. Lee, S. H. Lee, K. W. Choi, S. H. Choi. Association of ABCB1

718 polymorphisms with the efficacy of ondansetron for postoperative nausea and vomiting. Anaesthesia.
719 65 (10) (2010) 996–1000. https://doi.org/10.1111/j.1365-2044.2010.06476.x.

720 [45] H. Gréen, P. Söderkvist, P. Rosenberg, G. Horvath, C. Peterson. Mdr-1 single nucleotide
721 polymorphisms in ovarian cancer tissue: G2677T/A correlates with response to paclitaxel
722 chemotherapy. Clin. Cancer Res. 12 (3 I) (2006) 854–859. https://doi.org/10.1158/1078-0432.CCR-
723 05-0950.

724 [46] C. J. Chen, J. E. Chin, K. Ueda, D. P. Clark, I. Pastan, M. M. Gottesman, I. B. Roninson. Internal
725 duplication and homology with bacterial transport proteins in the Mdr1 (P-glycoprotein) gene from
726 multidrug-resistant human cells. Cell. 47 (3) (1986) 381–389. https://doi.org/10.1016/0092-
727 8674(86)90595-7.

728 [47] H. Omote, R. A. Figler, M. K. Polar, M. K. Al-Shawi. Improved energy coupling of human P-
729 glycoprotein by the glycine 185 to valine mutation. Biochemistry. 43 (13) (2004) 3917–3928.
730 https://doi.org/10.1021/bi035365l.

731 [48] A.R. Safa, R.K. Stern, K. Choi, M. Agresti, I. Tamai, N.D. Mehta, I.B. Roninson. Molecular
732 basis of preferential resistance to colchicine in multidrug-resistant human cells conferred by Gly-185
733 → Val-185 substitution in P-glycoprotein. Proc. Natl. Acad. Sci. U.S.A. 87 (18) (1990) 7225–7229.
734 https://doi.org/10.1073/pnas.87.18.7225.

735 [49] N. Harbeck, M. Gnant. Breast cancer. Lancet. 389 (10074) (2017) 1134–1150.
736 https://doi.org/10.1016/S0140-6736(16)31891-8.

737 [50] I. C. Salaroglio, E. Gazzano, A. Abdullrahman, E. Mungo, B. Castella, G. E. F. A. Abd-
738 elrahman, M. Massaia, M. Donadelli, M. Rubinstein, C. Riganti, J. Kopecka. Increasing intratumor
739 C/EBP-β LIP and nitric oxide levels overcome resistance to doxorubicin in triple negative breast

cancer. J. Exp. Clin. Cancer Res. 37 (1) (2018) 286. https://doi.org/10.1186/s13046-018-0967-0.

Figure Legends

Figure 1. Extraction procedure and structure of Glabratephrin.

Figure 2. MDA-MB-231/DX subline generation. MDA-MB-231 cells were cultured in medium with increasing concentration of Dox, as indicated in the Materials and methods section, generating the Dox-resistant subline (MDA/DX). **A.** At time 0 (p0) and every 5 passages (p), Pgp mRNA was measured by RT-PCR in triplicates. Parental MDA-MB-231 (MDA) cells were included as internal control. Data are presented as means ± SD (n=3). MDA-MB-231/DX cells vs. MDA-MB-231 cells: ** $p < 0.01$; *** $p < 0.001$. **B.** Cells were lysed and subjected to immunoblotting for the indicated proteins. Tubulin was used to check the equal protein loading. The figure is representative of 1 out of 3 experiments. **C.** Relative band density of Pgp, MRP1 and BCRP, performed with the ImageJ software. Data are presented as means ± SD (n=3). MDA-MB-231/DX cells vs. MDA-MB-231 cells: ** $p < 0.01$; *** $p < 0.001$. **D.** HIF-1α activity was measured by ELISA in duplicates. Data are presented as means ± SD (n=3). MDA-MB-231/DX cells vs. MDA-MB-231 cells: * $p < 0.05$; *** $p < 0.001$.

Figure 3. Doxorubicin accumulation and cytotoxicity in breast cancer cells with different degree of resistance. **A.** MDA-MB-231 cells (MDA), MDA-MB-231/DX cells (MDA/DX) and JC cells were lysed and subjected to immunoblotting for the indicated proteins. Tubulin was used to check the equal protein loading. The figure is representative of 1 out of 3 experiments. **B.** Relative band density of Pgp, MRP1 and BCRP, performed with the ImageJ software. Data are presented as means ± SD (n=3). MDA-MB-231/DX and JC cells vs. MDA-MB-231 cells: *** $p < 0.001$. **C.** Cells were incubated 24 h with 5 or 25 µM doxorubicin (Dox). The intracellular drug accumulation was

measured fluorimetrically in duplicates. Data are presented as means ± SD (n = 3). MDA-MB-231/DX cells vs. MDA-MB-231 cells: * $p < 0.05$; ** $p < 0.01$. **D.** Cells were grown 72 h in fresh medium (Ctrl) or in medium with 5 or 25 µM Dox. Cell viability was measured by crystal violet staining, in quadruplicates. Data are presented as means ± SD (n = 3). MDA-MB-231/DX cells vs. MDA-MB-231 cells: * $p < 0.05$; Dox vs Ctrl cells: °° $p < 0.01$, °°° $p < 0.001$.

Figure 4. Effects of Glabratephrin on doxorubicin cytotoxicity in breast cancer cells with different degree of resistance. **A-B-C.** MDA-MB-231 (MDA, panel **A**), MDA-MB-231/DX (MDA/DX, panel **B**) and JC (panel **C**) cells were grown for 72 h in fresh medium (0) or in medium containing Glabratephrin (Glab) at 1 nM, 10 nM, 100 nM, 1 µM and 10 µM, alone or in the presence of doxorubicin (Dox; 0.05 µM, 0.5 µM, 5 µM). Cell viability was measured by crystal violet staining in quadruplicates. The heatmaps represent the mean percentage of viable cells in each condition, in a colorimetric scale. The viability of untreated cells was considered 100% (n = 3 independent experiments). For MDA-MB-231 cells: Dox 0.05 µM vs. untreated cells: $p < 0.01$, Dox 0.5 and 5 µM vs. untreated cells: $p < 0.01$. For MDA-MB-231/DX cells: Dox 0.05, 0.5 and 5 µM vs. untreated cells: not significant; Dox + 10 nM Glab vs. Dox alone: $p < 0.05$; Dox + 100 nM/1 µM/10 µM Glab vs. Dox alone: $p < 0.001$. For JC cells: Dox 0.05, 0.5 and 5 µM vs. untreated cells: not significant; Dox + 100 nM Glab vs. Dox alone: $p < 0.05$; Dox + 1 µM/10 µM Glab vs. Dox alone: $p < 0.001$. **D-E.** MDA-MB-231/DX cells (MDA/DX, panel **D**) and JC cells (panel **E**) were grown for 72 h in fresh medium or in medium containing Dox and Glab, either alone or in combination, in the range of concentrations between 10^{-10} and10^{-5} M. Cell viability was measured by crystal violet staining in quadruplicates. The isobologram analyses were performed using the CalcuSyn software.

Figure 5. Effects of the combination of Glabratephrin and doxorubicin *in vivo*. JC cells were orthotopically implanted into 6-week-old female balb/C mice. When tumor reached the volume of 50

789 mm^3, mice (n= 8/group) were randomized and treated as reported in the following groups and treated
790 on day 1, 7, 14 after randomization as reported: 1) vehicle group (Ctrl), treated with 200 µl saline
791 solution intravenously (i.v.); 2) Glabratephrin group (Glab), treated with a 200 µl water/10% DMSO
792 solution i.v., containing 5 µM Glab; 3) doxorubicin group (Dox), treated with 5 mg/kg Dox, dissolved
793 in 200 µl water i.v.; 4) Glabratephrin + doxorubicin group (Glab+Dox), treated with 100 µl of saline
794 solution i.v. containing 5 µM Glab + 100 µl water solution containing 5 mg/kg Dox. **A.** Tumor
795 growth was monitored daily by caliper measurement. Data are presented as means ± SD. ***p<0.001:
796 Glab+Dox treatment vs all the other treatments (days 9-18). **B.** Photographs of representative tumors
797 of each group. **C.** Representative haematoxylin-eosin (HE) and Ki67 staining in each group of
798 treatments. For each experimental condition a minimum of 5 fields were examined. Ocular: 10X;
799 objective: 20X. **D.** Representative haematoxylin-eosin staining of liver, kidneys and spleen examined
800 *post-mortem* in each group of treatments. For each experimental condition a minimum of 5 fields
801 were examined. Ocular: 10X; objective: 10X (spleen), 20X (liver, kidneys).

802

803 **Figure 6.** Glabratephrin reduces Pgp activity. **A.** MDA-MB-231 cells (MDA), MDA-MB-231/DX
804 cells (MDA/DX) and JC cells were incubated 24 h with 5 µM doxorubicin (Dox), in the absence (-)
805 or presence (+) of 100 nM Glabratephrin (Glab). The intracellular drug accumulation was measured
806 fluorimetrically in duplicates. Data are presented as means ± SD (n = 3). Glab-treated vs. untreated
807 cells: * $p < 0.05$; *** $p < 0.001$. **B.** Cells were incubated 20 min with 1 µg/ml Rhodamine 123, in the
808 absence (-) or presence (+) of 100 nM Glab. The intracellular accumulation of Rhodamine 123 was
809 measured fluorimetrically in duplicates. Data are presented as means ± SD (n = 3). Glab-treated vs.
810 untreated cells: *** $p < 0.001$. **C.** Cells were incubated 10 min with increasing concentrations of Dox
811 (0.5-50 µM), in the absence (-) or presence (+) of 100 nM Glab. One series of dishes was analyzed
812 for the intracellular Dox concentration (c1); a second series was washed and let in the incubator for

additional 10 minutes, then analyzed for the intracellular Dox concentration (c2) as well. The dc/dt value was considered indicative of Dox velocity of efflux. Data are presented as means ± SD (n = 3). **D.** Cells were grown 24 h in the absence (-) or presence (+) of 100 nM Glab. The Pgp ATPase activity was measured specrophotometrically in duplicates. Data are presented as means ± SD (n = 3). Glab-treated vs. untreated cells: * $p < 0.05$; ** $p < 0.01$.

Figure 7. Docking of QZ59-RRR or Glabratephrin on Pgp. **A.** Superposition of the co-crystallized ligand QZ59-RRR (blue) and re-docked ligand QZ59-RRR (green) on Pgp (4M2S). **B.** Superposition of the co-crystallized ligand QZ59-RRR (blue) and Glabratephrin (green) on Pgp (4M2S). **C.** Putative binding mode of Glab with on Pgp (4M2S).

Figure 8. Modeling of the interactions between QZ59-RRR or Glabratephrin and Pgp**. A-B.** The functional groups involved in the interaction between QZ59-RRR (panel **A**) or Glabratephrin (panel **B**) and Pgp (4M2S) were displayed.

Figure 9. Glabratephrin loses its efficacy in Gly185Val mutated Pgp. MDA-MB-231 cells were transfected with an empty vector (mock) or with expression vectors encoding for wild-type (wt) Pgp, or Gly185Val, Ser400Asn, Gly412Ala, Ser893Ala, Ser893Thr-mutated Pgp. **A.** Cells were lysed and subjected to immunoblotting for Pgp. Tubulin was used to check the equal protein loading. The figure is representative of 1 out of 3 experiments. Numbers represent the relative band density of Pgp, calculated with the ImageJ software. **B.** Cells were incubated 24 h in the absence (-) or presence (+) of 100 nM Glabratephrin (Glab), with 5 µM doxorubicin (Dox). The intracellular drug accumulation was measured fluorimetrically in duplicates. Data are presented as means ± SD (n = 3). MDA-MB-231 cells overexpressing Pgp vs. mock cells: *** $p < 0.001$; Glab-treated cells vs corresponding untreated cells: °°° $p< 0.001$. **C.** The Pgp ATPase activity was measured spectrophotometrically in

duplicates. Data are presented as means ± SD (n = 3). MDA-MB-231 cells overexpressing Pgp vs. mock cells: *** $p < 0.001$; Glab-treated cells vs corresponding untreated cells: °°° $p < 0.001$.

Glabratephrin reverses doxorubicin resistance in triple negative breast cancer by inhibiting P-glycoprotein

Gamal-Eldein Fathy Abd-Ellatef[1,2], Elena Gazzano[1], Ahmed H. El-Desoky[3], Ahmed R. Hamed[4], Joanna Kopecka[1], Dimas Carolina Belisario[1], Costanzo Costamagna[1], Mohamed Assem S. Marie[5], Sohair R. Fahmy[5], Abdel-Hamid Z. Abdel-Hamid[2], Chiara Riganti[1,*]

[1]Department of Oncology, University of Torino, via Santena 5/bis, 10126, Torino, Italy

[2]Therapeutic Chemistry Department, Pharmaceutical and Drug Industries Research Division, National Re-search Centre, 33 El Bohouth St., 12622, Dokki, Giza, Egypt

[3]Pharmacognosy Department, Pharmaceutical and Drug Industries Research Division, National Research Centre, 33 El Bohouth St., 12622, Dokki, Giza, Egypt

[4]Chemistry of Medicinal Plants Department and Biology Unit of Central Laboratory, Pharmaceutical and Drug Industries Research Division, National Research Centre, 33 El Bohouth St., 12622, Dokki, Giza, Egypt

[5]Zoology Department, Faculty of Science, Cairo University, Gamaa Street, Giza, Egypt

[*]Correspondence: Dr. Chiara Riganti, Department of Oncology, University of Torino, via Santena 5/bis, 10126, Torino, Italy; email:chiara.riganti@unito.it; Phone: +390116705857; Fax: +390116705845

Supplementary Table S1. Effects of different concentrations of Glabratephrin on hematochemical parameters of the treated animals

	Ctrl	Glab 0.5 µM	Glab 1 µM	Glab 5 µM	Glab 10 µM
LDH (U/l)	6089 ± 609	6345 ± 451	6434 ± 509	6709 ± 709	9234 ± 789
AST (U/l)	236 ± 67	198 ± 48	221 ± 67	187 ± 59	509 ± 98 *
ALT (U/l)	35 ± 11	44 ± 8	41 ± 8	44 ± 11	58 ± 21*
AP (U/l)	109 ± 47	128 ± 46	117 ± 43	104 ± 34	171 ± 54
Creatinine (mg/l)	0.087 ± 0.013	0.096 ± 0.011	0.076 ± 0.012	0.085± 0.013	0.134± 0.012 *
CPK (U/l)	322 ± 65	267 ± 79	312 ± 68	334 ± 71	409 ± 103
CPK-MB (ng/ml)	0.127 ± 0.057	0.134 ± 0.056	0.098 ± 0.088	0.118 ± 0.095	0.138 ± 0.098
cTnI (pg/ml)	1.073 ± 0.045	1.103± 0.094	1.025 ± 0.058	1.075 ± 0.064	1.109 ± 0.067
cTnT (pg/ml)	2.195 ± 0.409	1.945 ± 0.398	2.329 ± 0.283	2.007 ± 0.368	1.893 ± 0.407

Balb/C mice (n=5 animals/group) were treated with vehicle (200 µl saline solution i.v., Ctrl) or with a 200 µl water/10% DMSO solution containing 0.5, 1, 5, 10 µM Glabratephrin (Glab) i.v. After 24 h animals were sacrificed, blood was collected and analyzed for lactate dehydrogenase (LDH), aspartate aminotransferase (AST), alanine aminotransferase (ALT), alkaline phosphatase (AP), creatinine, creatine phosphokinase (CPK) and CPK-MB, cardiac troponin I (cTnI) and T (cTnT). Data are presented as means ± SD. * $p < 0.05$: vs Ctrl group.

Supplementary Figures

Supplementary Figure S1

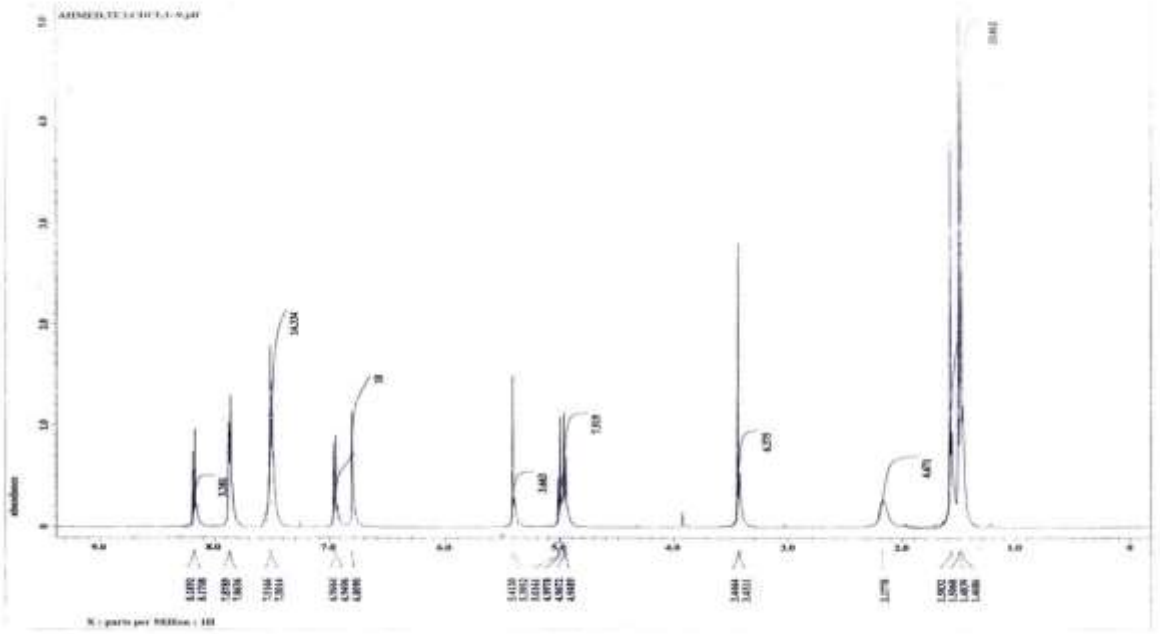

Figure S1. NMR spectrum of Glabratephrin (Pharmacognosy department in National Research Centre in Egypt).

Supplementary Figure S2

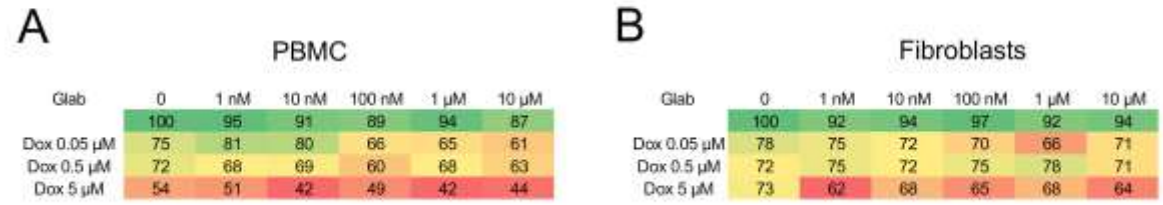

Figure S2. Effects of Glabratephrin and doxorubicin on non-transformed cells. Human peripheral blood mononuclear cells (PBMC, panel **A**) and human fibroblasts (panel **B**) were grown for 72 h in fresh medium (0) or in medium containing Glabratephrin (Glab) at 1 nM, 10 nM, 100 nM, 1 µM and 10 µM, alone or in the presence of doxorubicin (Dox, at 0.05 µM, 0.5 µM, 5 µM). Cell viability was measured by crystal violet staining in quadruplicates. The heatmaps represent the mean percentage of viable cells in each condition, in a colorimetric scale. The viability of untreated cells was considered 100%, (n = 3 independent experiments). For PBMC: Dox 0.5 µM vs. untreated cells: $p < 0.05$, Dox 5 µM vs. untreated cells: $p < 0.01$; Dox 0.05 µM + Glab 100 nM, 1 µM, 10 µM vs. untreated cells: $p < 0.05$; Dox 0.5 µM + Glab 1 nM, 10 nM, 100 nM, 1 µM, 10 µM vs. untreated cells: $p < 0.01$; Dox 5 µM + Glab 1 nM, 10 nM, 100 nM, 1 µM, 10 µM vs. untreated cells: $p < 0.001$. For fibroblasts: Dox 0.05 µM + Glab 1 µM: $p<0.01$; Dox 5 µM + Glab 1 nM, 10 nM, 100 nM, 1 µM, 10 µM vs. untreated cells: $p < 0.01$.

Supplementary Figure S3

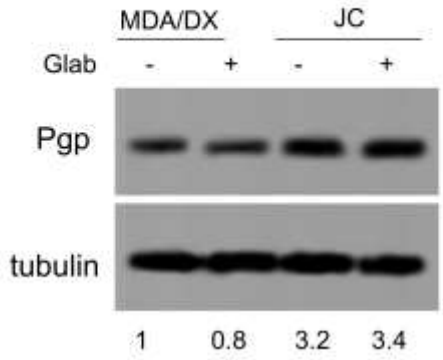

Figure S3. Expression of Pgp in cells incubated with Glabratephrin. MDA-MB-231/DX cells (MDA/DX) and JC cells were incubated in the absence (-) or in the presence of 100 nM Glabratephrin (Glab) for 24 h, then lysed and subjected to immunoblotting for Pgp. Tubulin was used to check the equal protein loading. The figure is representative of 1 out of 3 experiments. Numbers represent the relative band density of Pgp, calculated with the ImageJ software.

Supplementary Figure S4

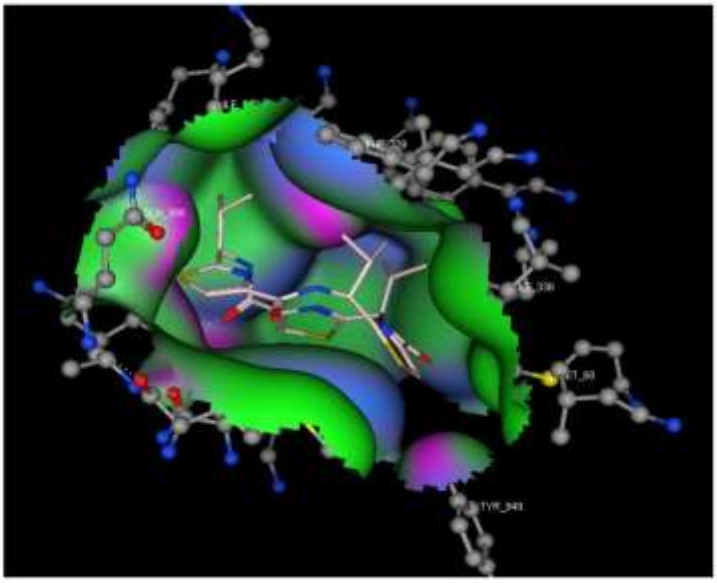

Figure S4. Docking simulation of QZ59-RRR to Pgp. Proposed model of interaction between QZ59-RRR and Pgp.